Topological Chaos in a Three-Dimensional Spherical Fluid Vortex

Spencer A. Smith[1,2], Joshua Arenson[2], Eric Roberts[2], Suzanne Sindi[2] and Kevin A. Mitchell[2]

[1] *Mount Holyoke College - South Hadley, MA 01075*
[2] *University of California Merced - Merced, CA 95343*

PACS 05.45.-a – Nonlinear dynamics and chaos
PACS 47.52.+j – Chaos in fluid dynamics
PACS 05.10.-a – Computational methods in statistical physics and nonlinear dynamics

Abstract – In chaotic deterministic systems, seemingly stochastic behavior is generated by relatively simple, though hidden, organizing rules and structures. Prominent among the tools used to characterize this complexity in 1D and 2D systems are techniques which exploit the topology of dynamically invariant structures. However, the path to extending many such topological techniques to three dimensions is filled with roadblocks that prevent their application to a wider variety of physical systems. Here, we overcome these roadblocks and successfully analyze a realistic model of 3D fluid advection, by extending the homotopic lobe dynamics (HLD) technique, previously developed for 2D area-preserving dynamics, to 3D volume-preserving dynamics. We start with numerically-generated finite-time chaotic-scattering data for particles entrained in a spherical fluid vortex, and use this data to build a symbolic representation of the dynamics. We then use this symbolic representation to explain and predict the self-similar fractal structure of the scattering data, to compute bounds on the topological entropy, a fundamental measure of mixing, and to discover two different mixing mechanisms, which stretch 2D material surfaces and 1D material curves in distinct ways.

Introduction. – The essential allure of chaotic dynamics is confronting a complex, seemingly random, physical process and discovering the hidden, underlying patterns that order it. This is typified by the seminal experiments of Gollub and Swinney, showing that the progression from regular to turbulent fluid flow occurs via the predictable period doubling cascade. [1] Immense success has been achieved in unraveling such patterns for chaotic systems reducible to maps on a one- or two-dimensional phase space [2–11]. A key theme in such studies is topological forcing: the existence of certain short-time structures (e.g. low-period orbits) forces the existence of infinitely many longer-time structures. The resulting patterns are typically fractal, with symbolic rules describing a rich self-similarity. Thus, early-time, low-resolution data predicts long-time, high-resolution patterns. This is nicely illustrated by the famous period-three-implies-chaos result: the existence of a single period-three orbit of a map on the unit interval guarantees the existence of periodic orbits of arbitrary period [2, 3]. A central challenge in dynamical systems then is to extend these topological techniques to higher dimensions, for which there are few clear paths forward [12–16].

In this paper, we demonstrate for the first time how chaotic scattering data for an explicit *three*-dimensional system, a numerical model of a chaotic time-periodic fluid vortex, reveals fractal rules of the dynamics. Our results follow from a deep topological understanding of special 2D surfaces within the fluid; the stable and unstable manifolds [17] attached to stagnation points. These manifolds intersect an infinite number of times in a beautiful fractal pattern called a heteroclinic tangle (Fig. 1**a**). We have developed a technique to extract the topology of the tangle in 3D from scattering data and turn it into a symbolic representation of the dynamics. We build on the understanding of heteroclinic tangles in 2D [6, 18–24], namely the homotopic lobe dynamics (HLD) technique [25–31]. A recent study [32] showed how to extend HLD to 3D for a few "tailor-made" tangles, absent any explicit dynamics. The key advances here are to demonstrate that this algorithm can be applied to a physically representative dynamical system that exists "in the wild" - passive advection in a modified Hill's spherical vortex, and to show that the resultant symbolic dynamics can be used to identify distinct stretching mechanisms and predict intricate fractal patterns in the scattering data.

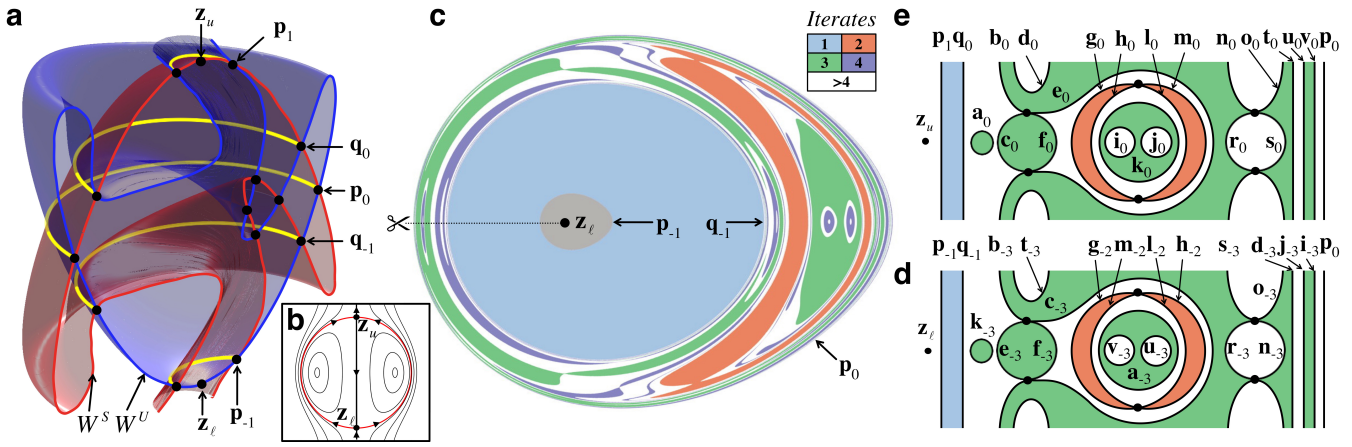

Fig. 1: **Hill's Vortex and Scattering Data.** **a**, 3D cut-away view of the modified Hill's vortex. **b**, Cross-sectional view of Hill's spherical vortex with streamlines. **c**, Numerically computed forward ETP. **d**, Cartoon of the forward ETP, with labeled intersection curves and dots indicating tangencies between W^U and W^S. This image can be constructed by cutting along the dotted line in **c** and folding all the topological information up, like a fan, into the rectangular region. **e**, Similar cartoon of the backward ETP. Reversibility guarantees that the forward and backward ETPs have the same pattern.

Chaotic spherical vortex. – Hill's vortex [33,34] is a well known solution to Euler's equations for an inviscid incompressible fluid, with stream-function

$$\psi(r,\theta) = \begin{cases} \frac{1}{2}U\left(1-\frac{a^3}{r^3}\right)r^2\sin^2\theta, & (r>a), \\ -\frac{3}{4}U\left(1-\frac{r^2}{a^2}\right)r^2\sin^2\theta, & (r<a), \end{cases} \tag{1}$$

where (r,θ) are the radius and azimuthal angle. The vortex radius is $a=1$, and the flow speed takes the uniform value $U=-1.2573$ far from the vortex. The velocity field in cylindrical coordinates is $\dot{\rho} = -\rho^{-1}\partial\psi/\partial z$ and $\dot{z} = \rho^{-1}\partial\psi/\partial\rho$. This flow has two unstable stagnation points (fixed points), $\mathbf{z}_u$ and $\mathbf{z}_\ell$, connected by a 2D spherical separatrix, separating the vortex interior from its exterior (Fig. 1**b**). The separatrix prevents mixing between fluid inside and outside the vortex. To induce mixing, we modify Hill's vortex by a sequence of time-periodic adjustments to the flow. We first create a map, H, by integrating an initial point (x,y,z) over the time interval $[0,1]$, using the velocity field derived from Eq. (1). Next we compose H with a series of maps, each used to break a particular symmetry. To break the separatrix, we use the map, $L_z(x,y,z) = \left(x,y,z+\epsilon\left(x^2+y^2\right)\right)$, with $\epsilon = 0.75$. To break the z-rotational symmetry, we apply a y-rotation, $R_y(\theta)$, with position-dependent rotation angle, $\theta(r) = 2\pi\delta_y(a-r)/\left(1+r^2\right)$, where $\delta_y = 0.3$. Finally, we use a z-rotation, $R_z(\theta)$, with $\theta(r) = 2\pi\delta_z(a-r)/\left(1+r^2\right)$, where $\delta_z = 0.2$. We then define the *advection map* as $M \equiv R_z^{-1}\circ R_y\circ L_z\circ H\circ L_z\circ R_y\circ R_z$. The resulting M is volume-preserving with fixed points $\mathbf{z}_u = (0,0,1)$ and $\mathbf{z}_\ell = (0,0,-1)$. It also satisfies $M^{-1} = S\circ M\circ S$, where $S(x,y,z) = (x,y,-z)$, i.e. reversing time is equivalent to reflecting about the xy-plane.

The advection map can be interpreted as evolving an initial point (x,y,z) forward one period under a time-periodic flow. The separatrix in Fig. 1**b** splits into two distinct surfaces, the 2D unstable manifold W^U of $\mathbf{z}_\ell$ and the 2D stable manifold W^S of $\mathbf{z}_u$ (Fig. 1**a**). (The stable/unstable manifold consists of all points that converge upon $\mathbf{z}_u/\mathbf{z}_\ell$ in forward/backward time.) These two manifolds first intersect at the primary intersection curve, $\mathbf{p}_0$, defining the unstable cap $W^U[\mathbf{p}_0]$, the piece of the unstable manifold between $\mathbf{z}_\ell$ and $\mathbf{p}_0$, and stable cap $W^S[\mathbf{p}_0]$. The vortex interior is the region between the stable and unstable caps. An intersection curve, e.g. $\mathbf{p}_0$, maps forward and backward to other intersection curves, e.g. $\mathbf{p}_1$ and $\mathbf{p}_{-1}$ (Fig. 1**a**).

HLD, from scattering data to symbolic dynamics. – Due to the broken separatrix, some advected particles outside the vortex will enter the vortex and subsequently escape. We treat this as a scattering problem (Fig. 1**c**), where the two impact parameters identify an initial point on the unstable cap, restricted to the domain $W^U[\mathbf{p}_{-1},\mathbf{p}_0]$ between $\mathbf{p}_{-1}$ and $\mathbf{p}_0$. The forward escape-time plot (ETP), Fig. 1**c**, is the number of iterates required to escape the vortex as a function of impact parameters. It is comprised of *escape domains*, which escape at a given iterate, surrounded by *gaps*, which have yet to escape. The *backward* ETP is defined analogously on $W^S[\mathbf{p}_0,\mathbf{p}_1]$ moving backward in time. Fig. 1**d** is a clearer-to-read cartoon of the forward ETP up to iterate 3; Fig. 1**e** is the backward ETP. Each boundary of the forward ETP eventually maps to a boundary of the backward ETP, as indicated by the subscripts. The ETPs constitute the input data for the HLD analysis. [32] Here we give a brief summary of how the analysis proceeds. The algorithm is detailed in Ref. [32].

The unstable manifold is partitioned into pieces, called *bridges*, by cutting along the stable cap. Each bridge

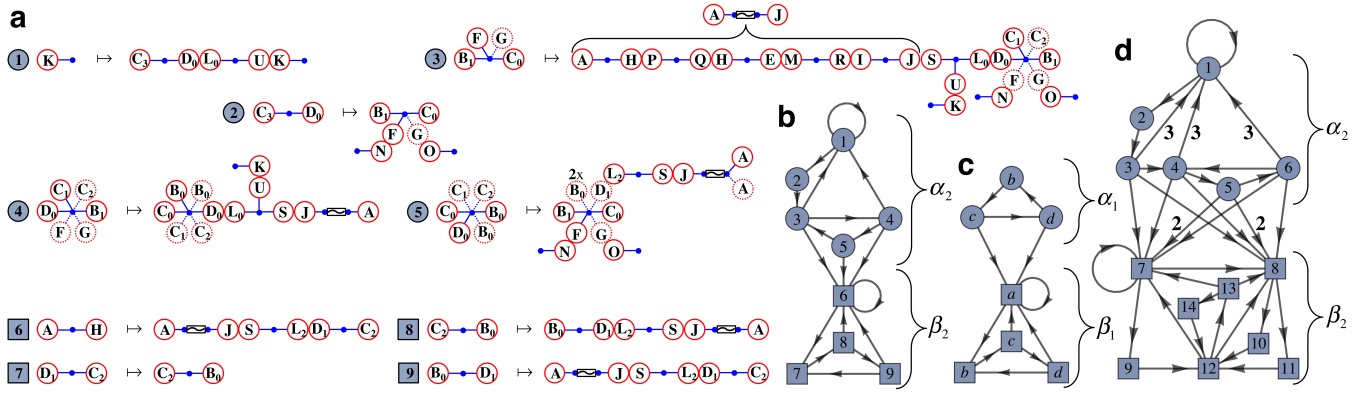

Fig. 2: **Symbolic Dynamics. a**, The active recurrent bridge classes and their iterates. Boundary classes marked with a dotted circle represent *inert* boundary classes. Bridge classes are considered equivalent if they only differ by inert boundary classes, for example bridge classes with boundaries $[[B_1, F, G, C_0]]$ and $[[B_1, F, G, C_0, D_1, B_0, B_0]]$. **b**, Transition graph for the 2D bridge classes in **a**. **c**, The 1D bridge class dynamics where α_1/β_1 1D bridge classes are embeddable in α_2/β_2 2D bridge classes. **a-c** represent the symbolic dynamics from iterate-three data. **d**, shows the 2D bridge class transition graph for the dynamics from iterate-four data.

is specified by the collection of curves that make up its boundary with the stable cap. Up to a given iterate of the unstable cap, the topology of each bridge and how bridges connect together can be reconstructed using the data in the forward and backward ETPs. The topology of this part of the tangle can be enforced by a set of systematically chosen obstruction rings. When placed in the 3D phase space, these obstruction rings act as impediments to pulling bridges through the stable cap, thereby preserving the topological complexity of the tangle. Obstruction rings partition the set of bridges into equivalence classes. Two bridges are of the same homotopy class, or *bridge class*, if one can be continuously deformed into the other without passing through an obstruction ring. These bridge classes form the central symbolic objects in our analysis, and their behavior under iteration constitutes a symbolic dynamical system.

Bridge classes can be specified by the homotopy classes, or *boundary classes*, of their boundary curves. This motivates the "barbell" pictograms of Fig. 2**a** as useful graphical representations of bridge classes. The labeled circles represent the boundary classes, and the lines connecting them represent the bridge class itself. Evolving forward one period, each bridge class maps to a set of bridge classes, glued together at their common boundaries (Fig. 2**a**). The algorithm produces a set of bridge classes that is closed under iteration, and excludes bridge classes that are transient (non-recurrent under the dynamics) or inert (map to exactly one bridge class after repeated iteration). This set and their relationships under the mapping, Fig. 2**a**, constitute the output data of the HLD analysis. The graph in Fig. 2**b** records the allowed transitions between bridge classes. The graph can also be presented as a transition matrix, $\mathbf{A}$, where A_{ij} is the number of directed edges connecting vertex j to vertex i.

The HLD analysis can be repeated for 1D bridges, paths beginning and ending on the stable cap and embedded in a 2D bridge. These 1D bridges are grouped into 1D bridge classes based on how they wrap around the obstruction curves. The forward iterates of 1D bridge classes can be obtained by iterating the 2D bridge classes in which they are embedded. Fig. 2**c** shows the transition graph of the resulting symbolic dynamics.

Topological entropy and stretching rates. – The vortex mixing is quantified by its topological entropy, which measures the exponential growth rate of "distinguishable" orbits as a function of time [35,36]. Intimately related is the topological entropy of the symbolic dynamics, or symbolic entropy — the log of the largest eigenvalue of $\mathbf{A}$. Since the symbolic dynamics represent the minimal topology forced by our knowledge of the tangle, its symbolic entropy is a lower bound to the full topological entropy of the advection map. Importantly, we can systematically increase this lower bound by including ETP data at successively higher iterates. In this study, data up to iterate three (Fig. 2**b**) gives a symbolic entropy of $\ln(1.6956)$, while the extra data at iterate four (Fig. 2**d**) increases this to $\ln(2.1106)$. For comparison, we directly computed the full topological entropy to lie between $\ln(2.7114)$ and $\ln(2.8210)$ using an independent approach [37], confirming our symbolic calculation as a lower bound.

Topological entropy also measures the maximum exponential stretching rate of material advected in the fluid. The symbolic entropies of the graphs in Figs. 2**b** and 2**c** give lower bounds on the stretching rates of 2D material surfaces and 1D material lines, respectively. Differing 2D and 1D stretching rates are possible for the 3D HLD analysis, (see ref. [32]). However, in this example the 1D and 2D stretching rates are *both* $\ln(1.6956)$ for the iterate-three analysis and $\ln(2.1106)$ for the iterate-four analysis.

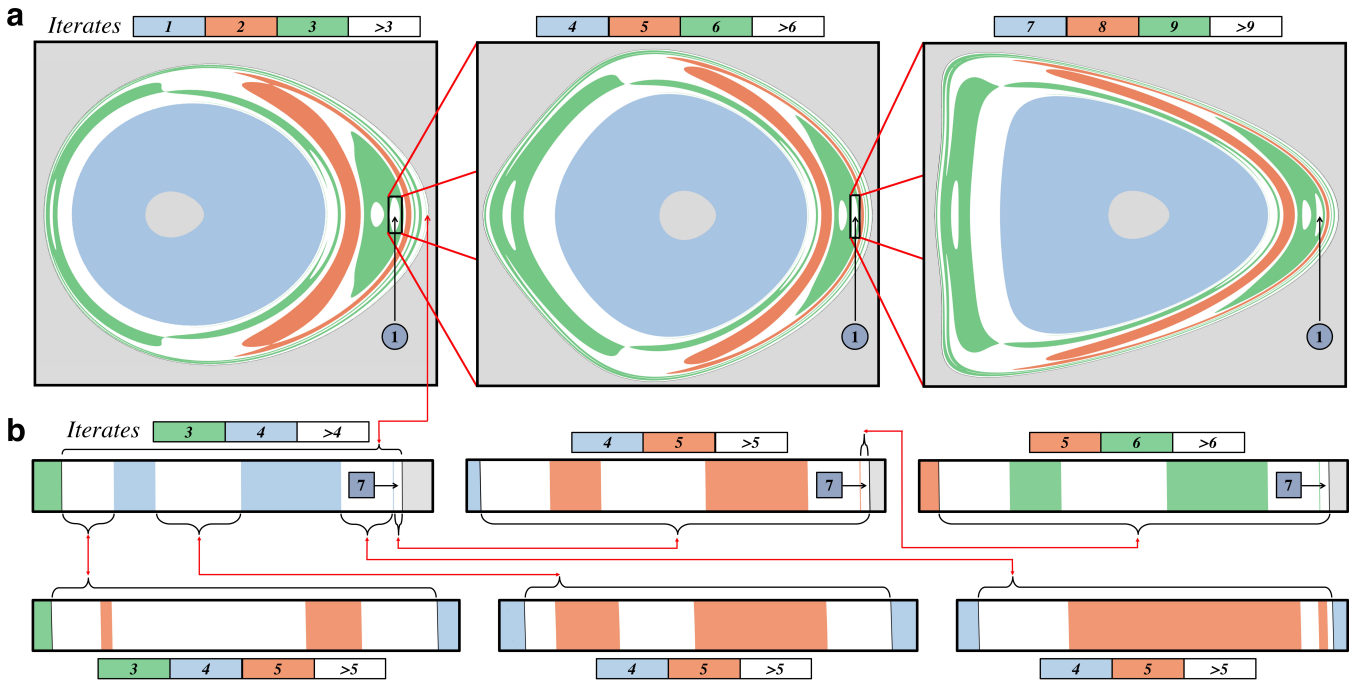

Fig. 3: **Fractal Structure** Numerical self-similar fractal regions. **a**, A complicated, fundamentally 2D, fractal structure. **b**, The three boxes on the top row each show three annular bands which repeat indefinitely upon zooming into the right-most gap, described by symbol 7 in Fig. 2**d** (which is the iterate-four-analysis analogue of symbol 6 in Figs. 2**a-c**). In the bottom row, from left to right, the minimal number of iterate-five escape domains forced by iterate-four knowledge are 0, 0, and 2. The extra observed escape domains in the first two bottom boxes illustrate that the actual structure can be more complicated than the forced structure, and that higher-iterate information should be included in the analysis to enlarge the forced dynamics.

The equality of these rates reflects a deep structural similarity between the 1D and 2D stretching mechanisms, as discussed next.

Two stretching mechanisms. – The transition graph (Fig. 2**b**) has two strongly connected components (SCCs), labeled α_2 and β_2. Each SCC represents a distinct stretching mechanism: The β_2 mechanism stretches material in one dimension, while the α_2 mechanism stretches material in two dimensions. To see this, note that each bridge in the β_2 SCC is a simple tube (with two boundary components), which is stretched out along its axis to multiple tubes under iteration, as seen in equations 6-9 of Fig. 2**a**, where each barbell is mapped to a chain of barbells. These tubes can thus be identified with the 1D bridge classes that run down their lengths, as reflected in the corresponding vertices of the β_2 and β_1 SCCs of Figs. 2**b** and 2**c**. However, the bridge classes in α_2 have a varied number of boundary components. Furthermore, there are only three distinct 1D bridge classes embedded in the 2D bridges of α_2, forming the α_1 SCC of Fig. 2**c**. But α_1 has zero symbolic entropy, whereas α_2 does not, meaning that all of the α_2 entropy generates fully 2D stretching. For example, symbol 1 in α_2 represents caps that are pushed down against the unstable cap $W^U[\mathbf{p}_0]$ in the z-direction, and stretched radially outward, away from the lower fixed point, in x and y. This fundamentally 2D behavior is also reflected in equations 1-5 of Fig. 2**a**, which exhibit branching not possible for 1D stretching. These two stretching mechanisms exist in the iterate-four dynamics as well (Fig. 2**d**).

While α_2 and β_2, differ in the dimensionality of their stretching, their symbolic entropies are identical. More tellingly, when taken as formal symbolic dynamical systems, i.e. bi-infinite shifts, we discovered a strong shift equivalence between α_2 and β_2, implying that their dynamics are topologically equivalent [38, 39]. These facts hold at iterate four as well. We conjecture that this equivalence is due to an underlying duality between forward-time 1D dynamics and backward-time 2D dynamics.

Fractal structure. – We started with scattering data in the ETPs, from which we derived a symbolic dynamics. Conversely, we can use the full symbolic dynamics to reconstruct the ETPs. More importantly, we used the symbolic dynamics represented by Fig. 2**d** to predict new, topologically-forced, escape domains at higher iterates. We then validated these predictions against direct numerical computations of the ETP at higher iterates. We focused on closed cycles in the transition graph, which generate fractal self-similar patterns in the ETP. Each symbol represents a motif in the fractal ETP — every gap labeled by that symbol will contain the same motif at higher iterates. For example, consider the 3-cycle $1 \to 2 \to 3$ in Fig. 2**d**. Every symbol "1" generated upon traversing this cycle once corresponds to a gap in each of the three panels of Fig. 3**a**. Zooming into this gap replicates this motif ad infinitum. Since this cycle is within the α_2 stretching mechanism, the associated motif is fundamentally 2D. Contrast this with the 1-cycle of 7 repeated within the β_2 stretching mechanism (Fig. 2**d**), whose associated motif is in the top three boxes of Fig. 3**b**. This motif is essentially 1D. In both Fig. 3**a** and Fig. 3**b**, the symbolic dynamics predict the exact fractal structure in the numerical ETPs. Note that iterate-four information was needed to produce such accurate symbolic dynamics, demonstrating the necessity —and power— of folding in new information at higher iterates. Indeed, at iterate five and higher, escape domains exist that are not predicted by iterate-four knowledge, e.g. the lower row of Fig. 3**b** shows extra, unpredicted bands at iterate five. Aside from being beautiful manifestations of the complexity inherent in the vortex, our fractal analysis demonstrates the important idea that finite knowledge of the scattering data forces the existence of an infinite succession of predictable structures in the tangle and ETPs.

Conclusions. – Successfully extending the 2D HLD technique to 3D paves the way for a structural characterization of the chaotic dynamics of other volume-preserving systems, like charged particles following magnetic field lines, shifting granular media, as well as many other 3D fluid flows. Furthermore, the HLD technique is algorithmic and amenable to automation. This would enable much higher iterates to be analyzed and also permit analyses of bifurcating mixing mechanisms. Finally, this current work is a spring-board to further extending the HLD technique to 4D symplectic maps derived from three-degree-of-freedom Hamiltonian systems, opening up many more applications, e.g. to chaotic atomic and molecular scattering.

* * *

We acknowledge Haik Stepanian for preliminary work on computing stable and unstable manifolds, and Bryan Malfeyt for initial discussions. We also thank Roy Goodman, Jacek Wróbel, Hector Lomeli, and Jason Mireles James for extensive discussions on computing these manifolds. This work was supported in part by the US DOD, ARO grant W911NF-14-1-0359 under subcontract C00045065-4.

REFERENCES

[1] Gollub J. P. and Swinney H. L., *Phys. Rev. Lett.*, **35** (1975) 927. http://link.aps.org/doi/10.1103/PhysRevLett.35.927

[2] Li T.-Y. and Yorke J. A., *American mathematical monthly*, (1975) 985.

[3] Sharkovskii A. N., *Ukrainian Math. J.*, **16** (1964) 61.

[4] Milnor J. and Thurston W., *On iterated maps of the interval* in *Dynamical systems (College Park, MD, 1986–87)* Vol. 1342 of *Lecture Notes in Math.* (Springer, Berlin) 1988 pp. 465–563.

[5] Thurston W. P., *Bull. Amer. Math. Soc. (N.S.)*, **19** (1988) 417.
[6] Easton R. W., *Trans. Am. Math. Soc.*, **294** (1986) 719.
[7] Boyland P., *Topol. Appl.*, **58** (1994) 223.
[8] Bestvina M. and Handel M., *Topology*, **34** (1995) 109.
[9] Gilmore R. and Lefranc M., *The Topology of Chaos: Alice in Stretch and Squeezeland* 2nd Edition (Wiley-Interscience) 2011.
[10] Boyland P. L., Aref H. and Stremler M. A., *J. Fluid Mech.*, **403** (2000) 277.
[11] Thiffeault J.-L. and Finn M. D., *Phil. Trans. A*, **364** (2006) 3251.
[12] Lefranc M., *Phys. Rev. E*, **74** (2006) 035202.
[13] Lefranc M., Morant P.-E. and Nizette M., *Philosophical Transactions of the Royal Society of London A: Mathematical, Physical and Engineering Sciences*, **366** (2008) 559.
[14] Jung C., Merlo O., Seligman T. H. and Zapfe W. P. K., *New Journal of Physics*, **12** (2010) 103021.
[15] Drótos G., González Montoya F., Jung C. and Tél T., *Phys. Rev. E*, **90** (2014) 022906.
[16] Drótos G. and Jung C., *Journal of Physics A: Mathematical and Theoretical*, **49** (2016) 235101.
[17] Wiggins S., *Chaotic Transport in Dynamical Systems* (Springer-Verlag, New York) 1992.
[18] Easton R., *Geometric Methods for Discrete Dynamical Systems* (Oxford University Press, New York) 1998.
[19] Rom-Kedar V., *Nonlinearity*, **7** (1994) 441.
[20] Rückerl B. and Jung C., *J. Phys. A*, **27** (1994) 55.
[21] Jung C. and Emmanouilidou A., *Chaos*, **15** (2005) 023101.
[22] Collins P., *Dynamics forced by surface trellises* in *Geometry and topology in dynamics* Vol. 246 of *Contemp. Math.* (Amer. Math. Soc., Providence, RI) 1999 pp. 65–86.
[23] Collins P., *International Journal of Bifurcation and Chaos*, **12** (2002) 605.
[24] Collins P., *Dyn. Syst.*, **19** (2004) 1.
[25] Mitchell K. A., Handley J. P., Knudson S. K. and Delos J. B., *Chaos*, **13** (2003) 892.
[26] Mitchell K. A. and Delos J. B., *Physica D*, **221** (2006) 170.
[27] Mitchell K. A., *Physica D*, **238** (2009) 737.
[28] Mitchell K. A., *Physica D: Nonlinear Phenomena*, **241** (2012) 1718 .
[29] Sattari S., Chen Q. and Mitchell K. A., *Chaos*, **26** (2016) .
[30] Novick J. and Delos J. B., *Phys. Rev. E*, **85** (2012) 016206.
http://link.aps.org/doi/10.1103/PhysRevE.85.016206
[31] Byrd T. A. and Delos J. B., *Phys. Rev. E*, **89** (2014) 022907.
http://link.aps.org/doi/10.1103/PhysRevE.89.022907
[32] Maelfeyt B., Smith S. A. and Mitchell K. A., *SIAM Journal on Applied Dynamical Systems*, **16** (2017) 729.
[33] Hill M. J. M., *Philosophical Transactions of the Royal Society of London. A*, **185** (1894) 213.
http://www.jstor.org/stable/90670
[34] Moffatt H. K. and Moore D. W., *J. Fluid Mech.*, **87** (1978) 749.
[35] Bowen R., *Transactions of the American Mathematical Society*, **154** (1971) 377.
http://www.jstor.org/stable/1995452
[36] Young L.-S., *Entropy in dynamical systems* in proc. of *Entropy* (Princeton University Press Princeton, NJ) 2003 pp. 313–327.
[37] Hunt B. R. and Ott E., *Chaos*, **25** (2015) .
http://scitation.aip.org/content/aip/journal/chaos/25/9/10.1063/1.4922973
[38] Lind D. and Marcus B., *An introduction to symbolic dynamics and coding* (Cambridge University Press, Cambridge) 1995.
http://dx.doi.org/10.1017/CBO9780511626302
[39] Kitchens B. P., *Symbolic dynamics* Universitext (Springer-Verlag, Berlin) 1998 one-sided, two-sided and countable state Markov shifts.
http://dx.doi.org/10.1007/978-3-642-58822-8